AIAA JOURNAL
Vol. 49, No. 1, January 2011

Tone Noise Prediction of a Propeller Operating in Nonuniform Flows

J. Xie* and Q. Zhou†
Huazhong University of Science and Technology, 430033 Wuhan, People's Republic of China
and
Philip F. Joseph‡
University of Southampton, Southampton, England SO17 1BJ, United Kingdom

DOI: 10.2514/1.J050423

This paper examines the tone noise generation by propellers operating in a nonuniform mean flow. A numerical approach is proposed, based in the frequency domain, for predicting far-field propeller noise, which requires the aerodynamic sources to be integrated over the actual blade surface, rather than over the mean-chord surface. The prediction of the radiated far-field tonal noise for a four-bladed propeller operating in a nonuniform mean flow is performed. Validation of the method is presented through a detailed comparison between numerical predictions of the far-field noise and the measured data, in which excellent agreement is obtained, both in magnitude and directivity. This paper concludes that for first harmonic noise, matching the number of the main inflow harmonic of nonuniform flow with blade number creates a dipole-type symmetric directivity pattern, and mismatching appears as an asymmetric directivity pattern. Effects of a single inflow harmonic on the far-field radiated tonal noise are also quantified in this paper, which shows that when the matching condition is satisfied, the main inflow harmonic contributes most of the total radiated sound pressure, except at locations normal to the propeller axis. When the matching condition is not satisfied, however, the total radiated sound pressure is mainly caused by the dominant inflow harmonic and the inflow harmonic that equals the blade number.

Nomenclature

A	=	complex amplitude of inflow harmonic
B	=	blade number
c	=	chord length of blade section
c_0	=	speed of sound
E	=	$R + M\,(y_1 - x_1)$
G	=	Green function in the time domain
$\bar{G}$	=	Green function in the frequency domain
H_0	=	zero-order Hankel function
H_1	=	first-order Hankel function
J	=	Bessel function
$\bar{k}_{n,r_0}$	=	nondimensional wave number of the nth velocity harmonic at radius r_0
$\bar{k}_x$	=	nondimensional wave number
l	=	radiated mode, indicating the order of blade-passing frequency
M	=	Mach number of the mean flow
$\mathbf{n}$	=	unit normal vector inward from the blade surface (n_1, n_r, n_θ)
n	=	order of inflow harmonic
P	=	pitch distance
R	=	mean-flow corrected distance
R_S	=	$\sqrt{x_1^2 + \beta^2 r^2}$
r	=	radial coordinate of observation point in the cylindrical coordinate system
r_0	=	radial coordinate of source point in the cylindrical coordinate system
t	=	time associated with arrival of sound wave at the observation point
U	=	inflow velocity
U_0	=	total incoming velocity at a propeller radius
u	=	axial inflow velocity
$\bar{u}$	=	circumferentially averaged axial mean velocity
$\tilde{u}$	=	axial disturbance velocity
V_x	=	absolute amplitude of inflow harmonic
$\mathbf{x}$	=	coordinates associated with the observation point; (x_1, r, θ') for cylindrical coordinates and (x_1, x_2, x_3) for the rectangular coordinate system
$\bar{x}$	=	nondimensional chord coordinate
$\mathbf{y}$	=	coordinates associated with the source point; (y_1, r_0, θ_0') for cylindrical coordinates and (y_1^b, y_2^b, y_3^b) for the rectangular coordinate system
α	=	attack angle at a blade radius section, $\gamma - \beta_H$
β	=	$\sqrt{1 - M^2}$
β_H	=	hydrodynamic pitch angle
γ	=	geometric pitch angle
δ	=	Dirac delta function
θ	=	azimuthal angle of observation point in the blade-fixed cylindrical coordinate system
θ_0	=	azimuthal angle of source point in the blade-fixed cylindrical coordinate system
κ	=	acoustic wave number related to the observation frequency ω, ω/c_0
μ	=	κ/β^2
ρ_0	=	density of unsteady oncoming flow
τ	=	time shift between the moving reference frame and the blade-fixed coordinate system
ψ	=	$\cos^{-1}(x_1/R_S)$
Ω	=	propeller rotational speed
ω	=	observation frequency
ω_0	=	source frequency in the blade-fixed coordinate system

Received 26 January 2010; revision received 15 September 2010; accepted for publication 22 September 2010.

*Ph.D. Student, Ship Science Department, 717 Jie Fang Road, Hubei.
†Professor, Ship Science Department, 717 Jie Fang Road, Hubei.
‡Professor, Institute of Sound and Vibration Research, Highfield.

I. Introduction

PROPELLERS usually operate in nonuniform mean flows in which large-scale inflow distortions are present in addition to small-scale turbulence. The interaction of the blades with incoming inflow distortions creates a periodically fluctuating pressure on the blade surface, which then leads to the radiation of discrete tones at the

blade-passing frequency and higher harmonics [1]. The interaction of the blades with inflow turbulence, on the other hand, leads to a random blade loading that then radiates as broadband noise. In most cases, tonal noise from propellers contains a greater sound power level than the broadband noise component.

Since the 1970s there has been considerable interest in the prediction of aerodynamic noise using both empirical and theoretical methods [2–6]. Lowson and Ollerhead [7] presented a closed-form near-field and far-field solutions for the unsteady pressure due to source singularities in arbitrary motion. In addition, they provided analytical solutions for the far-field directivity of a propeller operating in nonuniform flows. Wright [8] examined the influence of discrete frequency noise radiation due to periodic variations in the mean flow by employing a modal approach. He concluded that different types of wakes can produce tonal noise radiation; meanwhile, their amplitudes and directivities could have great discrepancies. The characteristics of the nonuniform flow upstream of a propeller are therefore critical to the accurate prediction of propeller tone noise radiation.

Heller and Widnall [9] analyzed the rotor–stator interaction noise of an axial compressor. By representing the unsteady blade forces with equivalent dipoles, they developed an analytical solution for rotor tonal noise prediction in which good agreement was obtained between experiment and theory. Blake [10] proposed a method for predicting the radiated tonal noise from a rotating propeller and concluded that at low-tip-speed Mach numbers the only inflow harmonics n that radiate sound are those for which $n = lB$, where l is the radiated mode, and B is the blade number. Thus, the propeller responds principally to those inflow harmonics that are multiples of the number of propeller blades. However, their models are restricted to integration of the source surface distribution on the mean-chord surface; the actual blade geometry is therefore neglected.

Recently, Seol et al. [11] numerically examined the thickness noise and loading noise of a marine propeller operating in nonuniform flows by using time-domain acoustic analogy. They concluded that monopole noise due to blade thickness is very small compared with the dipole noise. However, they did not reveal the relationship between nonuniform flows and unsteady blade surface pressure, and they did not discuss the effects of inflow harmonic number on the radiated noise.

As pointed out by Tyler and Sofrin [12], discrete tones are of generally much higher sound pressure level than the broadband noise component in nonuniform mean flows. Therefore, the prediction, and hence control, of propeller tone noise is important. Two important aspects must be addressed: one is to characterize the relationship between the nonuniform mean velocity field and unsteady blade pressure, and the other is to quantify variant effects of inflow harmonics.

Following the acoustic analogy, the classical approach in aeroacoustics is to represent the acoustic sources as an equivalent distribution of acoustic monopoles, dipoles, and quadrupoles. The strength of these sources is usually determined either experimentally or analytically. For most frequency-domain prediction methods, the source area of integration is mostly taken to be either on the projection disk or the blade mean-chord surface (e.g., Lowson and Ollerhead [7], Blake [10], Hanson [13], and Wojno et al. [14,15]).

The objective of the current research is to develop a frequency-domain numerical method for predicting far-field tonal noise of propellers operating in nonuniform flows by the use of the Green function solution to the acoustic analogy equations and that includes mean inflow effects. The new formulation and the numerical method presented are more important in situations in which the Mach number and the aerodynamic reduced frequencies are relatively small: say, marine propellers operating in nonuniform flows. The formulation provides clear insight into the mechanism of the generation of propeller tone noise. This prediction approach has the advantage that the source integration is performed on the actual blade surface, rather than on the projected disk or blade mean-chord surface. Numerical predictions of the tone noise level and directivity of a propeller operating in various nonuniform flows will be validated against existing experimental data. The various effects of a single inflow harmonic are quantified in this paper.

II. Coordinate Systems

The analysis presented here is formulated in a moving reference frame, which moves with the propeller at constant velocity $\mathbf{U} = (U, 0, 0)$, as shown in Fig. 1. In the moving reference frame, the coordinates of the observation point and the source point in a cylindrical coordinate system are denoted by $\mathbf{x} = (x_1, r, \theta')$ and $\mathbf{y} = (y_1, r_0, \theta_0')$, respectively. The relationships between the rectangular coordinate system and the cylindrical coordinate systems are

$$x_1 = x_1, \qquad x_2 = r\cos\theta', \qquad x_3 = r\sin\theta' \tag{1a}$$

$$y_1 = y_1, \qquad y_2 = r_0\cos\theta_0', \qquad y_3 = r_0\sin\theta_0' \tag{1b}$$

In both the translating and rotating blade-fixed coordinate systems, the observation point and the source point are denoted by $\mathbf{x}^b = (x_1, r, \theta)$ and $\mathbf{y}^b = (y_1, r_0, \theta_0)$, respectively. The transformations between the moving coordinate system and the blade-fixed coordinate system are

$$\mathbf{x}\,(x_1, r, \theta') = \mathbf{x}^b(x_1, r, \theta - \Omega\tau) \tag{2a}$$

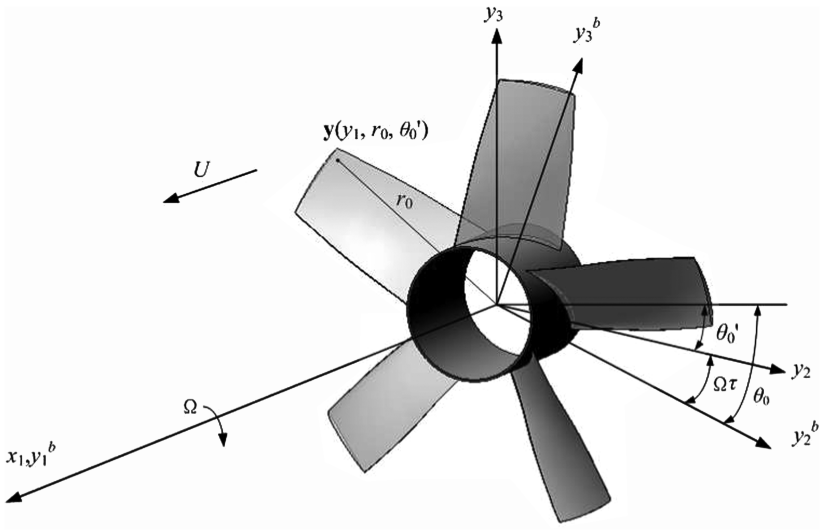

Fig. 1 Relation between the moving coordinate system and the blade-fixed coordinate system.

$$\mathbf{y}(y_1, r_0, \theta_0') = \mathbf{y}^b(y_1, r_0, \theta_0 - \Omega\tau) \tag{2b}$$

where τ is the time y shift between the moving coordinate system and the blade-fixed coordinate system, and Ω is the angular velocity of the blade rotating in the opposite direction of θ_0', as shown in Fig. 1.

III. Green Function Solution

The starting point for the prediction of propeller tonal noise is the Green function solution of the forced wave equation derived from the acoustic analogy. This is the fundamental equation governing the generation of aerodynamic sound in the presence of solid boundaries, whose Green function solution takes the form (for example, Goldstein [16])

$$p(\mathbf{x}, t) = \int_{-T}^{T} \iint_{v(\tau)} \int \frac{\partial^2 G}{\partial y_i \partial y_j} T_{ij}'(\mathbf{y}, \tau)\, \mathrm{d}\mathbf{y}\, \mathrm{d}\tau + \int_{-T}^{T} \iint_{S(\tau)} \frac{\partial G}{\partial y_i} f_i\, \mathrm{d}S(\mathbf{y})\, \mathrm{d}\tau + \int_{-T}^{T} \iint_{S(\tau)} \rho_0 V_n' \frac{\mathrm{D}G}{\mathrm{D}\tau}\, \mathrm{d}S(\mathbf{y})\, \mathrm{d}\tau \tag{3}$$

where $f_i = -n_i(p - p_0) + n_j e_{ij}$ is the ith component of the force per unit area exerted by the boundaries on the fluid, T_{ij}' is Lighthill's stress tensor for isotropic flow in a region $v(\tau)$, V_n' is the normal velocity on the blade surface $S(\tau)$, the primes on T_{ij}' and V_n' indicate the quantities observed in the earth-fixed reference frame, T is some large but finite interval of time, and $G = G(\mathbf{x}, t; \mathbf{y}, \tau)$ is the Green function of the wave equation relating to a medium with uniform mean flow. This Green function in an unbounded medium is given by (for example, Zhou and Joseph [17])

$$G(\mathbf{x}, t; \mathbf{y}, \tau) = \frac{1}{4\pi R} \delta\left[\tau + \frac{1}{\beta^2 c_0}(R + M(y_1 - x_1)) - t\right] \tag{4}$$

where $\beta^2 = 1 - M^2$, $M = U/c_0$ is the Mach number of the mean flow, and R is the mean-flow corrected distance:

$$R = \sqrt{(y_1 - x_1)^2 + \beta^2[r^2 + r_0^2 - 2rr_0\cos(\theta_0 - \Omega\tau - \theta')]} \tag{5}$$

We shall make use of the Green function in the frequency domain, which takes the form of

$$\bar{G}(\mathbf{x}, \mathbf{y}, \omega) = \int_{-\infty}^{\infty} G(\mathbf{x}, t; \mathbf{y}, \tau) e^{i\omega(t-\tau)}\, \mathrm{d}t = \frac{1}{4\pi R} e^{i\mu E} \tag{6}$$

where ω is the angular frequency, $E = R + M(y_1 - x_1)$, $\mu = \kappa/\beta^2$, and $\kappa = \omega/c_0$ is the acoustic wave number related to the observation frequency ω.

IV. Nonuniform Velocity Field

The characteristics of the noise due to the interaction of a propeller with mean inflow distortions are highly sensitive to the details of inflow velocity field upstream of the propeller; therefore, its description is extremely important. Experiments have shown that the inflow mean velocity at the propeller plane varies along the blade radius [18], which usually takes the smallest value at the hub and the highest value at the tip. Apart from the mean inflow velocity, there exist velocity disturbances in three directions. It may be easily demonstrated that the axial velocity component is most important in determining the radiated noise. It affects not only the noise level and directivity, but also the mechanism of the radiated noise.

The axial inflow velocity at point (r_0, θ_0) in the moving coordinate system can be described by the sum of a mean velocity component and an axial disturbance velocity of the form

$$u(r_0, \theta_0) = \bar{u}(r_0) + \tilde{u}(r_0, \theta_0) \tag{7}$$

where $\bar{u}(r_0)$ is the circumferentially averaged axial mean velocity at radius r_0, defined by

$$\bar{u}(r_0) = \frac{1}{2\pi} \int_0^{2\pi} u(r_0, \theta_0)\, \mathrm{d}\theta_0 \tag{8}$$

and $\tilde{u}(r_0, \theta_0)$ is axial disturbance velocity, which can be represented in terms of a Fourier series:

$$\tilde{u}(r_0, \theta_0) = \sum_{n=1}^{\infty} A_n(r_0) e^{-in\theta_0} \tag{9}$$

where $A_n(r_0)$ is the nth harmonic complex velocity amplitude at radius r_0.

V. Unsteady Blade Surface Pressure

Model a given radial section of the propeller as a linear cascade of airfoils, located at particular radius r_0, moving tangentially with respect to the freestream flow direction. If we consider a cylinder of radius r_0 cut through the propeller blade with cylinder axis coaxial with the propeller axis, the blade-section profile will closely fit on the cylinder surface. Unwrapping the cylinder surface onto a flat plane forms a right-angled triangle, as shown in Fig. 2. The adjacent side of the triangle is the circumference $2\pi r_0$, of the cylinder circular end. The opposite side is the advanced distance (pitch distance) P, parallel to the cylinder axis that a point would cover moving along the helicoidal chord line during one revolution. The hypotenuse of the triangle forms part of the blade-section chord line. The angle formed between the adjacent and the hypotenuse sides is referred to as the geometric pitch angle γ. Another right-angled triangle arises from the velocity triangle formed from the propeller forward velocity U and the blade-section rotating velocity Ωr_0. The total incoming velocity U_0 is therefore given by

$$U_0 = \sqrt{U^2 + (\Omega r_0)^2} \tag{10}$$

From this velocity triangle, as shown in Fig. 2, the hydrodynamic pitch angle can be obtained by

$$\beta_H = \tan^{-1}(U/\Omega r_0) \tag{11}$$

and the attack angle at the blade section is given by

$$\alpha = \gamma - \beta_H \tag{12}$$

The blade section samples each harmonic wave spatially and temporally as it spins. A fluctuating pressure field around the propeller is therefore produced. To fully account for the pressure distribution on the blade section, strip theory will be used. The unsteady blade response to each velocity harmonic will be estimated using the Sears unsteady aerodynamic theory.

However, it must be noted that the Sears analysis assumes the inflow disturbance to be normal to the blade section, in the blade-fixed reference frame. To apply Sears analysis to more general flow conditions, the normal component of the disturbance must be obtained. For a blade section, the unsteady pressure is antisymmetric [19]; that is, the pressures on the pressure and suction side of the blade are equal in magnitude, but π out of phase. Therefore, the unsteady pressure distribution on one side of the blade section can be expressed as [10]

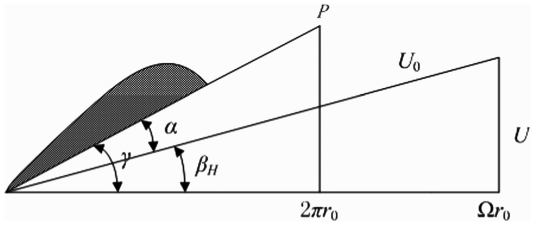

Fig. 2 Geometric pitch triangle and hydrodynamic velocity triangle.

$$p(r_0,\theta_0;\tau)=\rho_0 U_0(r_0)\cos\gamma(r_0)\sum_{n=1}^{\infty}A_n(r_0)e^{-in\theta_0'}\mathrm{Sears}(\bar{k}_{n,r_0}) \tag{13}$$

Note that the pressure distribution is the summation of contributions made by all harmonic waves, where (r_0,θ_0) represents the local coordinates evaluated in the blade-fixed reference frame, $\gamma(r_0)$ represents the geometric pitch angle at radius r_0, $U_0(r_0)$ represents the mean inflow velocity at radius r_0, as shown in Fig. 2, and $\bar{k}_{n,r_0}$ is the nondimensional wave number of the nth velocity harmonic normalized by half-chord at that particular radius r_0.

Note that $\mathrm{Sears}(\bar{k}_{n,r_0})$ in Eq. (13) is the product of Sears transfer function and the chord distribution, defined by

$$\mathrm{Sears}\,(\bar{k}_x)=\mathrm{Se}(\bar{k}_x)\sqrt{\frac{1-\bar{x}}{1+\bar{x}}} \tag{14}$$

where $\bar{k}_x$ is the nondimensional wave number (reduced frequency), and $\bar{x}$ represents the nondimensional chord coordinates, which takes the value of $[-1, 1]$ from the leading edge to the trailing edge. The classical Sears aerodynamic transfer function $\mathrm{Se}(\bar{k}_x)$ for a two-dimensional vertical gust in an incompressible fluid is defined as

$$\mathrm{Se}\,(\bar{k}_x)=\frac{2i}{\bar{k}_x\pi}\left[\frac{1}{H_1^{(2)}(\bar{k}_x)+iH_0^{(2)}(\bar{k}_x)}\right] \tag{15}$$

where H_0 and H_1 represent the zero-order and the first-order Hankel functions, respectively.

VI. Tonal Noise Radiation

Note that the first term in Eq. (3) represents the quadrupole source contribution and the third term represents the volume displacement source. These terms are only found to be important at relative flow speeds close to the sound speed [20]. Therefore, when considering the sound radiation due to the interaction between rotating blades and large-scale nonuniformities, only the second term of Eq. (3) is of importance, which is denoted by

$$p(\mathbf{x},t)=\int_{-T}^{T}\iint_{S(\tau)}\frac{\partial G}{\partial y_j}f_j\,\mathrm{d}S(\mathbf{y})\,\mathrm{d}\tau \tag{16}$$

Substituting the Green function of Eq. (6) into Eq. (16) and Fourier-transforming the result with respect to t, one obtains the radiated pressure for a single blade surface S_i at observer frequency ω of the form

$$\hat{p}(\mathbf{x},\omega)=\frac{1}{2\pi}\int_{-T}^{T}\iint_{S_i}f_j(\mathbf{y},\tau)e^{i\omega\tau}\frac{\partial}{\partial y_j}\bar{G}(\mathbf{x},\mathbf{y})\,\mathrm{d}S(\mathbf{y})\,\mathrm{d}\tau \tag{17}$$

To simplify the analysis, the following far-field approximations are made: r_0 and $y_1\ll R_s$, where $R_s=\sqrt{x_1^2+\beta^2r^2}$ is the flow corrected distance from the origin of the blade-fixed reference system to the observation point. It is natural to express the observation point in the moving reference frame, whereas the source point is expressed in the blade-fixed coordinate system; hence, only the time-shift variable τ appears inside the expression of R and R_s. Expanding the expression of R and ignoring terms of second order gives

$$R\approx R_s-[y_1\cos\psi+\beta^2r_0\sin\psi\cos(\theta_0'-\theta')] \tag{18}$$

where $\cos\psi=x_1/R_s$ and $\sin\psi=r/R_s$. Note that ψ is not a geometric angle; in terms of the small value of Mach number, it can be regarded approximately as an azimuthal angle measured from the x_1 axis. With the approximate expression for R of Eq. (18) and the derivatives $\partial/\partial y_i$ of the Fourier transform of the Green function substituted into Eq. (17), one obtains

$$\begin{aligned}\hat{p}(\mathbf{x},\omega)=&\frac{-i\mu}{8\pi^2}\frac{e^{i\mu R_s}}{R_s}\int_{-T}^{T}\iint_{S_i}\{-f_T(y,\tau)[(y_1-x_1)/R_s+M]\\&+f_R(y,\tau)\beta^2[-r_0/R_s+\sin\psi\cos(\theta_0'-\theta')]\\&-f_D(y,\tau)\beta^2\sin\psi\sin(\theta_0'-\theta')\}\\&\times e^{i\omega\tau}e^{i\mu M(y_1-x_1)}e^{-i\mu[y_1\cos\psi+\beta^2r_0\sin\psi\cos(\theta_0'-\theta')]}\,\mathrm{d}S(y)\,\mathrm{d}\tau\end{aligned} \tag{19}$$

where f_T, f_R, and f_D denote the forces per unit area exerted by the propeller blades in the y_1, r_0, and θ_0 directions, respectively. Here, the usual far-field approximation is made, whereby $1/R$ is replaced by $1/R_s$. The forces in Eq. (19) are related to the blade surface pressure of Eq. (13) by

$$\begin{Bmatrix}f_T\\f_R\\f_D\end{Bmatrix}=-\begin{Bmatrix}n_1\\n_r\\n_\theta\end{Bmatrix}p(r_0,\theta_0;\tau) \tag{20}$$

where $\mathbf{n}=\{n_1,n_r,n_\theta\}$ is the normal vector pointing inward from the blade surface.

Substituting the unsteady blade surface pressure distribution $p(r_0,\theta_0;\tau)$ of Eq. (13) into Eqs. (19) and (20) gives

$$\begin{aligned}\hat{p}(\mathbf{x},\omega)=&\frac{-i\mu\rho_0}{8\pi^2}\frac{e^{i\mu R_s}}{R_s}\int_{-T}^{T}\iint_{S_i}\left\{n_1\left[\frac{y_1-x_1}{R_s}+M\right]\right.\\&\left.-n_r\beta^2\left[-\frac{r_0}{R_s}+\sin\psi\cos(\theta_0'-\theta')\right]+n_\theta\beta^2\sin\psi\sin(\theta_0'-\theta')\right\}\\&\cdot\sum_{n=1}^{\infty}A_n(r_0)e^{-in(\theta_0-\Omega\tau)}U_0(r_0)\mathrm{Sears}(\bar{k}_{n,r_0})\\&\times\cos\gamma(r_0)e^{i\omega\tau}e^{i\mu M(y_1-x_1)}e^{-i\mu[y_1\cos\psi+\beta^2r_0\sin\psi\cos(\theta_0'-\theta')]}\,\mathrm{d}S(y)\,\mathrm{d}\tau\end{aligned} \tag{21}$$

Ignoring the effects on the radiated sound field from scattering of sound by adjacent blades, summing over B blades, and following a similar procedure to [21], the final expression for the total radiated noise is obtained of the form

$$\begin{aligned}\hat{p}(\mathbf{x},\omega)=&\frac{-i\mu B\rho_0}{4\pi R_s}e^{i\mu(R_s-Mx_1)}\\&\times\sum_{l=-\infty}^{\infty}\sum_{n=1}^{\infty}e^{i(lB-n)(\theta'-\frac{\pi}{2})}\delta(\omega+lB\Omega)\iint_{S_i}\left\{n_1\left[\frac{y_1-x_1}{R_s}+M\right]\right.\\&-n_r\beta^2\left[-\frac{r_0}{R_s}+i\sin\psi\left(\frac{lB-n}{\kappa r_0\sin\psi}-\frac{J_{lB-n+1}(\kappa r_0\sin\psi)}{J_{lB-n}(\kappa r_0\sin\psi)}\right)\right]\\&\left.-n_\theta\beta^2\frac{lB-n}{\kappa r_0}\right\}J_{lB-n}(\kappa r_0\sin\psi)A_n(r_0)U_0(r_0)\\&\times\cos\gamma(r_0)e^{i\mu(M-\cos\psi)y_1}e^{-ilB\theta_0}\mathrm{Sears}(\bar{k}_{n,r_0})\,\mathrm{d}S(\mathbf{y}^b)\end{aligned} \tag{22}$$

where l represents the number of radiated harmonic noise order, which takes all integer values, n is the number of inflow velocity harmonic order, and $\delta(\omega+lB\Omega)$ denotes a Dirac delta function evaluated at frequencies shifted by the blade-passing frequencies $lB\Omega$. Note that Eq. (22) requires integration to be performed over the actual blade surface $S(\mathbf{y}^b)$, rather than over the mean-chord surface. The term of $n_1[(y_1-x_1)/R_S+M]$ in Eq. (22) is a very important parameter. This component accounts for the influence of the unsteady axial force on the radiated noise; furthermore, it can be easily reduced to $-\cos\psi+M$ in the far-field condition, where y_1 is sufficiently small compared with the observation abscissa x_1. Thus, it can be used to evaluate the radiated far-field noise directivity. In addition, the prediction equation (22) includes the effects due to radial force and tangential force.

VII. Comparison of Tonal Noise Predictions with Experimental Data

In this section the theory developed above is compared against experimental data reported by Subramanian and Mueller [22]. Tonal

noise radiation measurements were made in an anechoic wind tunnel for a four-bladed propeller developed by the David Taylor Ship Research and Development Center. The propeller has an expanded area ratio of 0.451, a tip diameter of 0.2504 m, a hub-to-tip ratio of 0.2, and is coded as Prop 3714 in the U.S. Naval propeller listings. The main geometric parameters of the full-scale propeller can be found in [22]. The nonuniform flow was provided by with two separate flow generators, which produced a three or four-cycle sinusoidal velocity distribution. The measurements were made at propeller rotational speeds n of 3000 and 3600 rpm at freestream speeds U of 12.7 m/s. A single hot-wire sensor, mounted on a three-dimensional traversing unit, was employed for quantifying the nonuniform variation of the axial flow velocity. An array of microphones was used to measure the radiated far-field tonal noise directivity at a radius of 1.9 m on both sides of the propeller axis.

From the measured axial velocity data relating to the three-cycle and four-cycle flows, the harmonic variations V_x along a propeller radius given by Eq. (9) were computed. Figures 3 and 4 illustrate the main inflow harmonic variations along the propeller radius for the two different nonuniform flows.

Figure 3 shows the dominance of the third harmonic along the entire propeller radius. Although other velocity harmonics are also present in the flowfield, they are significantly weaker in magnitude. The amplitude of the third harmonic linearly increases with radius and reaches a value of 0.08 near the propeller tip. In Fig. 4, the amplitude of the fourth velocity harmonic is much higher than the other two harmonics. The maximum amplitude of the fourth harmonic is about 0.07 near the blade tip.

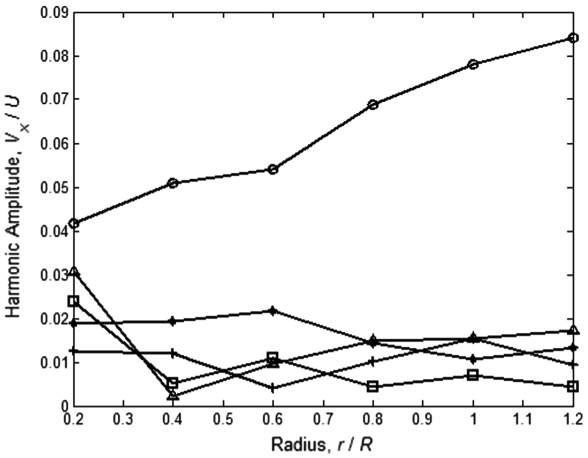

Fig. 3 Three-cycle flow: radial variation of the main inflow harmonics: △ harmonic 1, □ harmonic 2; ○ harmonic 3; * harmonic 4; + harmonic 5.

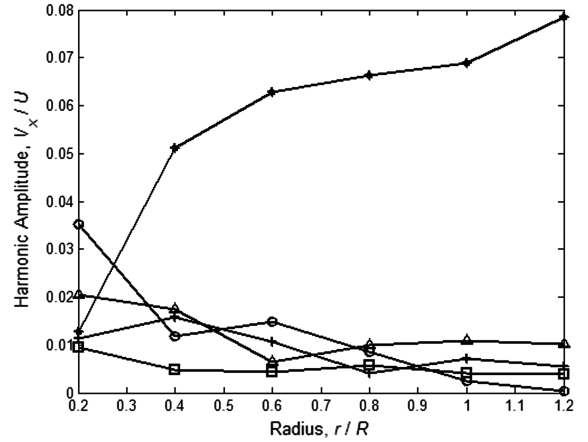

Fig. 4 Four-cycle flow: radial variation of the main inflow harmonics: △ harmonic 1, □ harmonic 2, ○ harmonic 3, * harmonic 4, and + harmonic 5.

A numerical scheme has been developed for the efficient computation of the radiated tonal noise at different observation points. The blade surface is meshed into triangle elements with a maximum dimension of 8–10 times less than the mean-flow reduced wavelength. This allows analytic integration over each element facet, whose integrand involves the oscillating terms in Eq. (22). Figure 5 shows a pressure-side mesh used to perform the numerical integration required in Eq. (22).

The unsteady blade loading, which constitutes the aerodynamic sound sources, is predicted using Eqs. (13–15). Substituting the unsteady blade loading into the tonal noise prediction equation (22) allows predictions of the radiated tonal noise to be obtained. As pointed out by Subramanian and Mueller [22], the first harmonic noise ($l = 1$) is much greater than the noise at higher harmonics [22]; thus, only the first harmonic noise is considered for comparison purposes. For the sake of comparison, the radiated tonal noise computed by the analytic solution proposed by Blake [10] is also presented.

Figure 6 shows a comparison of the first harmonic noise directivity ($l = 1$) for three-cycle flow at a propeller rotational speed 3000 rpm. The numerical prediction using the method proposed above is typically 2 dB greater than the measured sound pressure level at the 50° position, and between angles from 90 to 130°, the differences are less than 1 dB. A trend of smooth decrease in the tonal sound level from downstream to upstream is demonstrated. The prediction results of Blake's [10] analytic solution, however, deviate from the measured results, with a maximum difference of approximately 11 dB at 50°, which then diminishes as the observer angles increase. The downstream-to-upstream decreasing trend is not accurately captured by the Blake model.

Figure 7 shows a comparison of the first harmonic noise directivity for three-cycle flow at a propeller rotational speed 3600 rpm. The numerical predictions are observed to be even closer in level to the

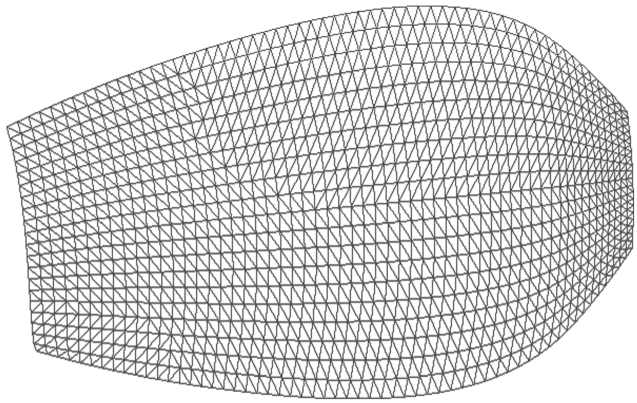

Fig. 5 Mesh for numerical calculation of 3714 propeller, pressure side.

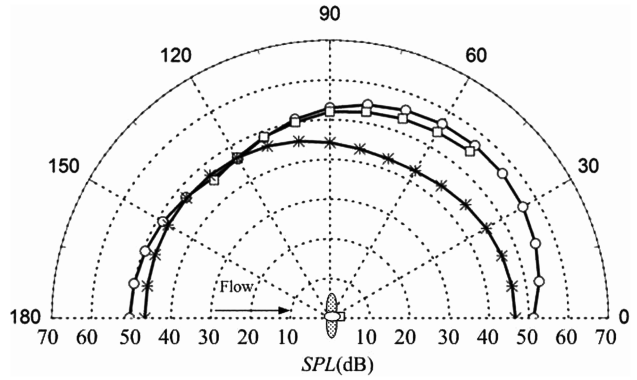

Fig. 6 Comparison of predicted and measured first harmonic directivities for three-cycle flow at propeller rotational speed 3000 rpm: ○ predicted, □ measured, and * Blake's analytic solution.

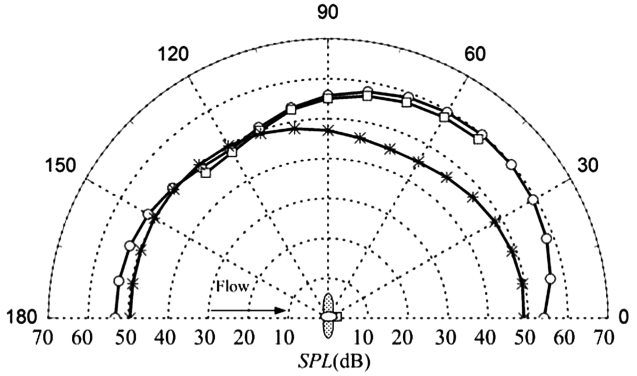

Fig. 7 Comparison of predicted and measured first harmonic directivities for three-cycle flow at propeller rotational speed 3600 rpm: ○ predicted, □ measured, and * Blake's analytic solution.

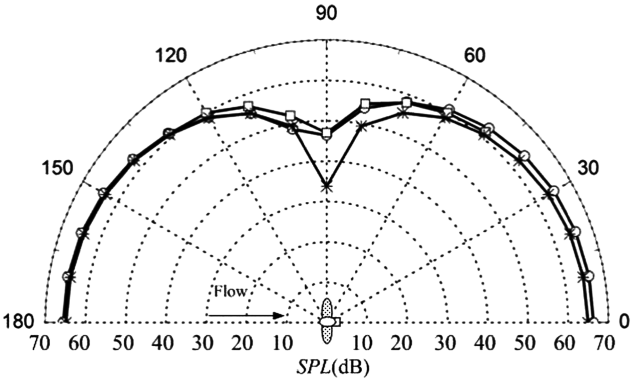

Fig. 9 Comparison of predicted and measured first harmonic directivities for four-cycle flow at propeller rotational speed 3600 rpm: ○ predicted, □ measured, and * Blake's analytic solution.

measured data at all nine measured points than those at the rotational speed of 3000 rpm. The maximum differences at this speed are no more than 1.5 dB. The variation in noise between downstream-to-upstream observer angles is again well-captured. The prediction of Blake [10] at this speed is in even poorer agreement, however, with a difference of 11.5 dB at 50°, and at 130°, it is slightly greater than the measured values, by 0.5 dB. It also fails to capture the downstream-to-upstream trend of diminishing level.

Figure 8 illustrates a comparison of the first harmonic noise directivity for four-cycle flow at a propeller rotational speed 3000 rpm. The numerical predictions show an excellent agreement with the measured data at angles between 50 to 90°, and at angles greater than 90°, the numerical predictions are lower than the measured values, with a maximum difference of about 6.3 dB at an angle of 100°. The minimum value is observed to be in the plane located at 90° and represents a plane of symmetry. Although the prediction obtained using Blake's [10] analytic solution also has symmetric features, it has a minimum value of up to 31.2 dB, which is typically 13.5 dB lower than the measured value at an angle of 90°.

As shown in Fig. 9, the directivity at 3600 rpm has symmetric features. The numerical predictions are even closer to the measured values than those at 3000 rpm. The differences between the numerical predictions and the measured data are within a scatter of 2 dB at all spherical locations, except at 100°, where the numerical prediction is about 3.2 dB less than the measured values. Blake's [10] analytic solution also predicts the same characteristics as those at 3000 rpm, with a minimum value of 33.8 dB, which is about 13.2 dB lower than measured values.

Comparing the sound pressure level directivity at the first harmonic for the three-cycle flow and the four-cycle flow at a propeller rotational speed of 3000 rpm, as illustrated in Figs. 6 and 8, a clear feature is that the radiated noise levels for four-cycle flow are higher than those of three-cycle flow, except in the direction normal to the propeller axis. This is most likely a result of the different coupling effects of the main inflow harmonic and the rotating blades.

Note that the numerical prediction, the measured results, and the predictions using Blake's [10] analytic solution for four-cycle flow appears as an axial dipole-type symmetric far-field directivity pattern. This radiation symmetry appears to be a direct result of the symmetry in the four-cycle mean velocity profile. From the tonal noise prediction formulation of Eq. (22) and the properties of the Bessel function, it can be deduced that the strongest inflow harmonic that couples with the rotating blades must satisfy the matching condition $lB - n = 0$. Therefore, in confining analysis to the first radiated harmonic noise ($l = 1$), one has $n = 4$. When the matching condition is satisfied (that is, the fourth inflow harmonic component is dominant in nonuniform flows), the influence due to radial force and tangential force can be neglected, and the axial force component $n_1[(y_1 - x_1)/R_S + M]$ can be reduced to $-\cos\psi$; thus, the prediction formula of Eq. (22) can be approximated as

$$[\hat{p}(\mathbf{x},\omega)]_{l=1} = \frac{-i\mu B\rho_0}{4\pi R_s} e^{i\mu(R_s - Mx_1)} \times \sum_{n=1}^{\infty} \iint_{S_i} n_1 \cos\psi J_0(\kappa r_0 \sin\psi) A_n(r_0) U_0(r_0) \times \cos\gamma(r_0) e^{i\mu(M-\cos\psi)y_1} e^{-iB\theta_0} \mathrm{Sears}(\bar{k}_{n,r_0})\, \mathrm{d}S(\mathbf{y}^b) \quad (23)$$

The zero-order Bessel function and the cosine function are even functions; therefore, the above approximation formula can be considered as an even function in terms of azimuthal angle ψ. This will lead to the result of an axial dipole-type symmetric directivity, due to strong coupling between the fourth inflow harmonic and the rotating blades, as illustrated in Figs. 8 and 9. As to Blake's [10] analytic solution, when the matching condition is satisfied, it can also be approximated as an even function in terms of azimuthal angle ψ; therefore, the corresponding result is a symmetric feature. For mismatching conditions ($lB - n \neq 0$), where the fourth harmonic is not significant, Eq. (22) cannot be approximated as an even function in terms of azimuthal angle ψ; consequently, the result is an asymmetry in directivity, due to weak coupling, as illustrated in Figs. 6 and 7.

The sound pressure level of each radiated harmonic noise is the sum of the interactions between all inflow velocity harmonics and the rotating blades. Therefore, quantifying various effects of a single inflow velocity harmonic on the radiated noise is important to the understanding of the mechanism of propeller tone noise, and this may further assist in the reduction of propeller noise.

The sound pressure level for a single inflow velocity harmonic is now investigated. Figure 10 shows the comparison of the predicted and single inflow harmonic directivities for the three-cycle flow at a propeller rotational speed of 3000 rpm. It is clear that the sound pressure level for inflow harmonic 3 makes the greatest contribution to the total radiated at angles between 40 to 130° and tends to zero along the propeller axis. At angles below 40° and above 130°,

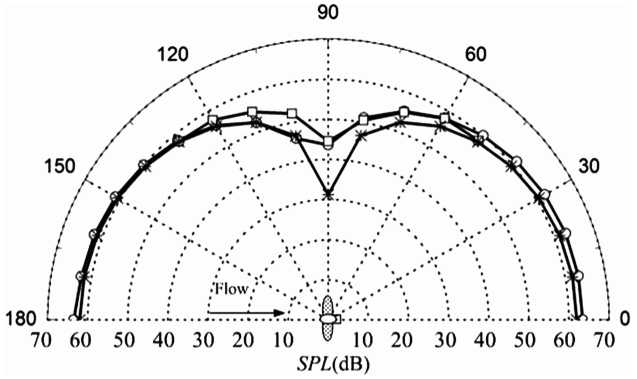

Fig. 8 Comparison of predicted and measured first harmonic directivities for four-cycle flow at propeller rotational speed 3000 rpm: ○ predicted, □ measured, and * Blake's analytic solution.

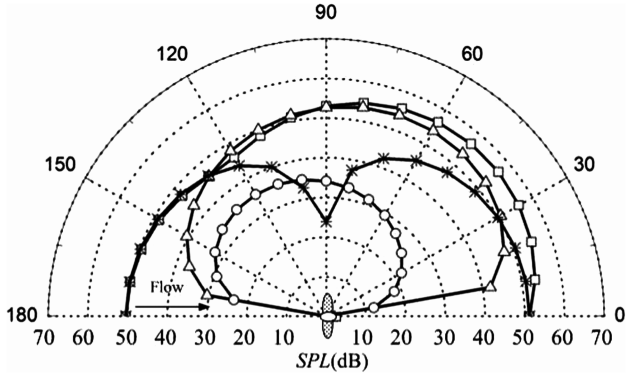

Fig. 10 Comparison of predicted and single harmonic directivities for three-cycle flow at propeller rotational speed 3000 rpm: □ total predicted, △ harmonic 3, * harmonic 4, and ○ harmonic 5.

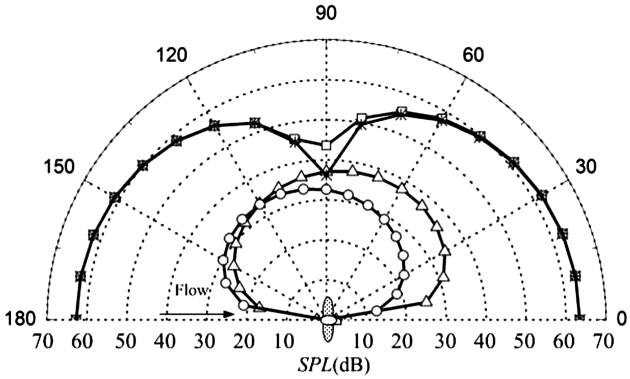

Fig. 11 Comparison of predicted and single harmonic directivities for four-cycle flow at propeller rotational speed 3000 rpm: □ total predicted, △ harmonic 3, * harmonic 4, and ○ harmonic 5.

however, the noise directivity for inflow harmonic 4 is closer to the total radiated noise than that for harmonic 3. Note that the inflow harmonic 3 is the main inflow harmonic under three-cycle flow conditions, as shown in Fig. 3. Therefore, it may be concluded that for mismatching conditions ($lB - n \neq 0$), the total radiated sound pressure level is mainly caused by two inflow harmonics: the main inflow harmonic and the inflow harmonic that satisfies $n = lB$. Furthermore, the sound pressure level for the main inflow harmonic dominates over most locations, except at locations near the propeller axis, and the inflow harmonic that satisfies $n = lB$ dominates at locations near the propeller axis.

Figure 11 shows the comparison of the predicted and single inflow harmonic directivities for four-cycle flow at a propeller rotational speed of 3000 rpm. The sound pressure level for harmonic 4 is extremely close to the total radiated at most of locations, except in the direction normal to the propeller axis. A symmetric directivity is also demonstrated. By contrast, the sound pressure levels for harmonic 3 and harmonic 5 are comparatively smaller at all locations and even tend to zero along the propeller axis. Note that in this symmetric flow, the inflow harmonic 4 is highly dominant everywhere, and thus the matching condition is satisfied. Therefore, for matching conditions, the total radiated sound pressure level is mainly determined by the inflow harmonic that satisfies $n = lB$, and a dipole-type symmetric directivity is obtained.

VIII. Conclusions

A numerical approach in the frequency domain has been described for predicting propeller far-field tonal noise in nonuniform mean flows. The integration of the surface sources for computation of the radiated sound field is evaluated on the actual propeller surface, rather than over the mean-chord plane.

An extensive comparison between the predicted sound pressure level with the measured data shows generally excellent agreement, both in magnitude and directivity. The numerical prediction shows a symmetric directivity for four-cycle flow and an asymmetric directivity for three-cycle flow. A numerical scheme aimed at predicting the sound pressure level for a single inflow velocity harmonic shows that when the matching condition $n = lB$ is satisfied, the main inflow harmonic contributes very dominantly to the total radiated sound pressure level, except at locations normal to the propeller axis. When the matching condition is not satisfied, however, the total radiated sound pressure level is mainly caused by the main inflow harmonic and the inflow harmonic that satisfies $n = lB$. The sound pressure level for the main inflow harmonic dominates over most of locations, except at locations near the propeller axis, and the inflow harmonic that satisfies $n = lB$ dominates at locations near the propeller axis. Acoustic predictions were also performed using a classical approach. The proposed formulation is shown to more closely match the experimental data, both for matching and mismatching conditions. The method will be used for parameter research of marine propeller noise due to interaction between the rotating blades and the nonuniform flows caused by upstream appendages.

References

[1] Morfey, L., "Rotating Blades and Aerodynamic Sound," *Journal of Sound and Vibration*, Vol. 28, No. 3, 1973, pp. 587–617. doi:10.1016/S0022-460X(73)80041-0

[2] Amiet, R. K., "Acoustic Radiation from an Airfoil in a Turbulent Stream," *Journal of Sound and Vibration*, Vol. 41, No. 4, 1975, pp. 407–420. doi:10.1016/S0022-460X(75)80105-2

[3] Paterson, R. W., and Amiet, R. K., "Noise of a Model Helicopter Rotor Due to Ingestion of Turbulence," NASA CR-3213, 1979.

[4] Woan, C. J., and Gregorek, G. M., "The Exact Numerical Calculation of Propeller Noise," 11th AIAA Fluid and Plasma Dynamics Conf., Seattle, WA, AIAA Paper 78-1122, 1978.

[5] Amiet, R. K., "Noise Produced by Turbulent Flow into a Propeller or Helicopter Rotor," 3rd AIAA Aeroacoustics Conf., Palo Alto, CA, AIAA Paper 76-560, 1976.

[6] Homicz, G. F., and George, A. R., "Broadband and Discrete Frequency Radiation from Subsonic Rotors," *Journal of Sound and Vibration*, Vol. 36, No. 2, 1974, pp. 151–177. doi:10.1016/S0022-460X(74)80292-0

[7] Lowson, M. V., and Ollerhead, J. B., "A Theoretical Study of Helicopter Rotor Noise," *Journal of Sound and Vibration*, Vol. 9, No. 2, 1969, pp. 197–222. doi:10.1016/0022-460X(69)90028-5

[8] Wright, S. E., "The Acoustic Spectrum of Axial Flow Machines," *Journal of Sound and Vibration*, Vol. 45, No. 2, 1976, pp. 165–223. doi:10.1016/0022-460X(76)90596-4

[9] Heller, H. H., and Widnall, S. E., "The Role of Fluctuating Forces in the Generation of Compressor Noise," NASA CR-2012, 1972.

[10] Blake, W. K., *Mechanics of Flow-Induced Sound and Vibration*, Academic Press, New York, 1986.

[11] Seol, H., Suh, J. C., and Lee, S., "Development of Hybrid Method for the Prediction of Underwater Propeller Noise," *Journal of Sound and Vibration*, Vol. 288, Nos. 1–2, 2005, pp. 345–360. doi:10.1016/j.jsv.2005.01.015

[12] Tyler, J. M., and Sofrin, T. G., "Axial Flow Compressor Noise Studies," *S.A.E. Transactions*, Vol. 70, 1962, pp. 309–332.

[13] Hanson, D. B., "Helicoidal Surface Theory for Harmonic Noise of Propellers in the Far Field," *AIAA Journal*, Vol. 18, No. 10, 1980, pp. 1213–1220. doi:10.2514/3.50873

[14] Wojno, J. P., Mueller, T. J., and Blake, W. K., "Turbulence Ingestion Noise, Part 1: Experimental Characterization of Grid-Generated Turbulence," *AIAA Journal*, Vol. 40, No. 1, 2002, pp. 16–25. doi:10.2514/2.1636

[15] Wojno, J. P., Mueller, T. J., and Blake, W. K., "Turbulence Ingestion Noise, Part 2: Rotor Aeroacoustic Response to Grid-Generated Turbulence," *AIAA Journal*, Vol. 40, No. 1, 2002, pp. 26–32. doi:10.2514/2.1637

[16] Goldstein, M. E., *Aeroacoustics*, McGraw–Hill, New York, 1976.

[17] Zhou, Q., and Joseph, P. F., "A Frequency Domain Numerical Method for Airfoil Broadband Self-Noise Prediction," *Journal of Sound and*

Vibration, Vol. 299, No. 3, 2007, pp. 504–519.
doi:10.1016/j.jsv.2006.06.061

[18] Shaw, L. M., and Balombin, J. R., "Rotor Wake Characteristics Relevant to Rotor-Stator Interaction Noise Generation," 7th AIAA Aeroacoustics Conf., Palo Alto, CA, AIAA Paper 81-2031, 1981.

[19] Minniti, R. J., and Mueller, T. J., "Influence of Proximity to a Solid Boundary on the Unsteady Loading of a Thin Airfoil," 6th AIAA/CEAS Aeroacoustic Conf. and Exhibit, Lahaina, HI, AIAA Paper 2000-1987, 2000.

[20] Gerard, A., Berry, A., and Masson, P., "Control of Tonal Noise from Subsonic Axial Fan. Part 1: Reconstruction of Aeroacoustic Sources from Far-Field Sound Pressure," *Journal of Sound and Vibration*, Vol. 288, Nos. 4–5, 2005, pp. 1049–1075.
doi:10.1016/j.jsv.2005.01.023

[21] Zhou, Q., and Joseph, P. F., "Frequency-Domain Method for Rotor Self-Noise Prediction," *AIAA Journal*, Vol. 44, No. 6, 2006, pp. 1197–1206.
doi:10.2514/1.16176

[22] Subramanian, S., and Mueller, T. J., "An Experimental Study of Propeller Noise Due to Cyclic Flow Distortion," *Journal of Sound and Vibration*, Vol. 183, No. 5, 1995, pp. 907–923.
doi:10.1006/jsvi.1995.0295

C. Bailly
Associate Editor